Title

Functional analysis and crystallographic structure of clotrimazole bound OleP, a cytochrome P450 epoxidase from *Streptomyces antibioticus* involved in Oleandomycin biosynthesis.

Funding Source Statement

We are grateful to synchrotrons ELETTRA (beamline 5.2R, XRD1, Trieste, Italy). The European Community - Research Infrastructure Action under the FP7/2007-2013 under grant agreement no 226716 is acknowledged.

Authors and Affiliations

Linda Celeste Montemiglio[1,+], Giacomo Parisi[1,+], Antonella Scaglione[1], Giuliano Sciara[2], Carmelinda Savino[3,*], Beatrice Vallone[1,3,*]

Istituto Pasteur-Fondazione Cenci Bolognetti and Istituto di Biologia e Patologia Molecolari del CNR, Dipartimento di Scienze Biochimiche "A. Rossi Fanelli", Sapienza Università di Roma, Piazzale A. Moro 5, 00185 Rome, Italy

[1]Department of Biochemical Sciences, "Sapienza" University of Rome, P.le A. Moro 5, 00185 Rome, Italy.

[2]Unité de Bioénergétique et Ingénierie des Protéines, Institut de Microbiologie de la Méditerranée, CNRS-UMR7281, Aix-Marseille Université, Marseille, France

[3]CNR Institute of Molecular Biology and Pathology, P.le A. Moro 5, 00185 Rome, Italy.

[+]Both authors contributed equally to this work.

*To whom correspondence should be addressed. E-mail: linda.savino@uniroma1.it; beatrice.vallone@uniroma1.it Telephone: +39 06 49910548. Fax: +39 06 4440062.

Abstract

BACKGROUND
OleP is a cyt P450 from *S. antibioticus* carrying out epoxigenation of the antibiotic oleandomycin during its biosynthesis. The timing of its reaction has not been fully clarified, doubts remain regarding its substrate and catalytic mechanism.

METHODS
The crystal structure of OleP in complex with clotrimazole, an inhibitor of P450s used in therapy was solved and the complex formation dynamics was characterized by equilibrium and kinetic binding studies and compared to ketoconazole, another azole differing for the N1-substituent.

RESULTS
Clotrimazole coordinates the heme and occupies the active site. Most of the residues interacting with clotrimazole are conserved and involved in substrate binding in MycG, the P450 epoxigenase with the highest homology with OleP. Kinetic characterization of inhibitor binding revealed OleP to follow a simple bimolecular reaction, without detectable intermediates.

CONCLUSIONS
Clotrimazole-bound OleP adopts an open form, held by a π-π stacking chain that fastens helices F and G and the FG loop. Affinity is affected by the interactions of the N1 substituent within the active site, given the one order of magnitude difference of the off-rate constants between clotrimazole and ketoconazole. Based on structural similarities with MycG, we propose a binding mode for both oleandomycin intermediates, that are the candidate substrates of OleP.

GENERAL SIGNIFICANCE
Among P450 epoxigenases OleP is the only one that introduces an epoxide on a non-activated C-C bond. The data here presented are necessary to understand the rare chemistry carried out by OleP, to engineer it and to design more selective and potent P450-targeted drugs.

Abbreviations and Textual Footnotes: [1]OleP, 8.8a-oleandolide epoxigenase; [2]P450, cytochrome P450; [3]EpoK, Epothilone C-D monooxygenase; [4]PimD, Pimaricin monooxygenase; [5]MycG, Mycinamicin monooxygenase; [6]CLT, clotrimazole; [7]KC, ketoconazole; [8]DMSO, dimethyl sulfoxide; [9]DEO, 8.8a-oleandolide; [10]LO-DEO, L-olyvosil-8.8a-deoxyoleandolide; [11]CTZ-OleP, OleP in complex with CTZ; [12]rmsd, root mean square deviation; [13]M-III, mycinamicin III; [14]M-IV, mycinamicin IV; [15]M-V, mycinamicin V; [16]i.s., ionic strength; [17]SEC, Size Exclusion Chromatography.

The atomic coordinates and the structure factors were deposited under the code 4XE3 (OleP, the cytochrome P450 epoxidase from *Streptomyces antibioticus* involved in Oleandomycin biosynthesis: functional analysis and crystallographic structure in complex with clotrimazole) in the Protein Data Bank Research Collaboratory for Structural Bioinformatics, Rutgers University, New Brunswick, NJ (http://www.rcsb.org).

Keywords: CYP107D1, P450, Epoxigenases, Oleandomycin, Clotrimazol and ketoconazole, Crystal structure

Introduction

Cytochrome P450s are heme-containing monooxygenases involved in a rich variety of functions such as the biosynthesis of many endogenous compounds (*i.e.* steroid hormones, vitamin D3, retinoic acid, prostaglandins, fatty acid derivatives, mycotoxins, macrolide antibiotics) and the biotransformation of drugs and xenobiotics that they perform in virtually all living systems.[1,2] These multifaceted catalysts promote the insertion of an atom of molecular oxygen into unactivated C-H or C-C bonds, generally in a regio- and stereo-selective manner.[3] One of the most peculiar aspects of their activity is that, depending on their physiological role, the same overall fold and a common mechanistic basis for catalysis are exploited to perform chemically different reactions on a plethora of alternative substrates. Due to this peculiarity P450s are considered the most versatile biological catalysts existing in nature.[1] The interest in understanding the molecular basis underlying the P450 versatility in drugs and xenobiotic detoxification as well as the strict substrate-, chemo-, regio- and stereo-specificity spans from the research of alternative drug targets both for antimicrobial therapy and for the treatment of metabolic disorders and cancer, to the identification of new members exhibiting biotechnological relevant properties. Presently, still very few chemical methods allow for direct monooxygenation of aliphatic or aromatic C-H bonds, which are also either not selective or with low efficiency. A major challenge in protein engineering is to use the powerful chemistry of P450s for applications in the field of bioremediation and in organic synthesis to produce libraries of new chemicals and drugs.[4,5]

The 8.8a-oleandolide monooxygenase, OleP, from the actinomycete *Streptomyces antibioticus* (CYP107D1), is a P450 epoxigenase involved in the biosynthesis of the 14-membered polyketide antibiotic, oleandomycin (Figure 1A).

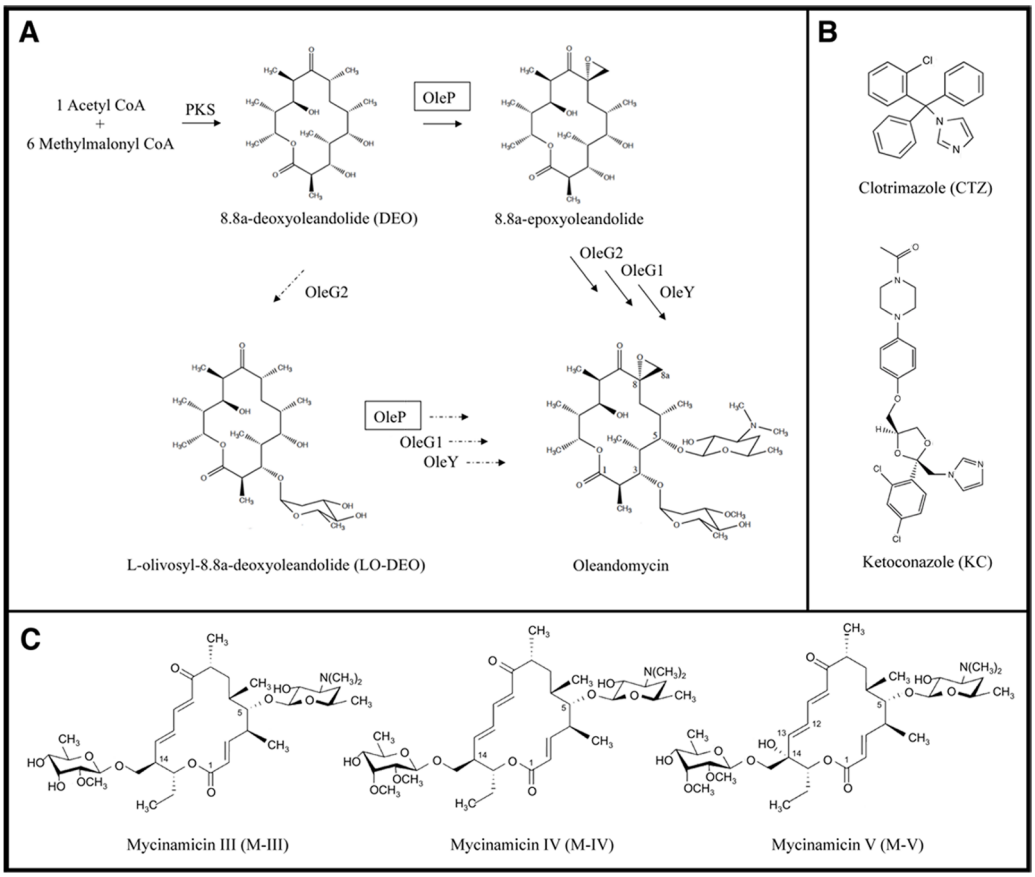

Figure 1. A. The biosynthetic pathway of Oleandomycin. Gaisser *et al.* [7] proposed that the process might proceed through two parallel pathways depending on the timing of the OleP reaction. Continuous arrows indicate the possible pathway if 8,8a-deoxyoleandolide (DEO) epoxidation is the first step, while dotted arrows show the sequence of biosynthetic steps in case L-olivosyl-8,8a-deoxyoleandolide (LO-DEO) is (or is also) the OleP substrate. **B. Chemical structures of the two azole antifungal compounds clotrimazole (CTZ) and ketoconazole (KC). C. Chemical structures of Mycinamycin III (M-III) and the two physiological substrates of MycG, Mycinamicin IV (M-IV) and Mycinamycin V (M-V).**[12]

The constitutive unit of the oleandomycin structure is the macrolactone ring. This intermediate is the product of a specific polyketide synthase complex that, during the first stage of the biosynthesis, assembles an acetate unit and six molecules of methylmalonyl CoA by means of sequential reactions of condensation and decarboxylation with a final thioesterase-driven cyclization. Afterwards, the aglicone moiety undergoes tailoring reactions that comprise the attachment of two 6-deoxysugars at C3 and C5, L-oleandrose and D-desosamine respectively, the former being methylated at the 3'-OH by a specific methyl tranferase, and a reaction of epoxidation that OleP catalyses in a regio- and stereo-specific manner at the C8-C8a of the macrolactone ring.[6]

The correct sequence of the events occurring during the tailoring phase of the process and involving the OleP reaction has not yet been fully clarified, since discordant findings have been to date reported.[7–10] For this reason, since its identification in 1995, OleP has been the object of studies focused on clarifying its physiological substrate. Nevertheless, given the paucity of structural and functional data *in vitro*, many doubts still remain regarding both the timing of the OleP reaction and the mechanism of epoxidation itself catalysed by this P450.

To date, four macrolide P450 epoxidases have been structurally and functionally characterized, most of them being multifunctional monooxygenases performing, together with epoxidation, stereospecific reaction of hydroxylation.[11–14] Among them, EpoK, PimD and MycG introduce the epoxide function directly on olefinic carbons. Remarkably, OleP is able to perform the epoxidation on aliphatic carbons, the C8 and C8a of the oleandomycin aglicone (Figure 1A), possibly proceeding through an olefinic intermediate generated by OleP itself.[7]

Here we present the crystallographic structure of the P450 OleP, obtained in complex with clotrimazole, a common P450 inhibitor widely used in the treatment of fungal diseases. Binding properties of OleP to clotrimazole has been investigated and compared to the OleP binding mechanism to another P450 inhibitor, ketoconazole, endowed with a more elongated and less bulky shape (Figure 1B). A detailed comparison with the structurally known P450 epoxigenases and the

relevance of this structure in the context of P450 inhibition and biotechnological usage as bio-catalyst will be discussed.

Materials and Methods

Cloning, Expression and Purification. The plasmid pSGOleP, a pUC18 cloning vector containing the nucleotide sequence coding for OleP [7,8], was kindly provided by Biotica Technology Ltd. The gene was extracted by restriction with NdeI and BgIII and inserted into the expression vector pET28b(+) under the same sites. This construct results in the expression of the protein sequence in frame with a hexa-histidine tag at its N-terminus, containing a thrombin cleavage site between the histidine tag and the OleP sequence. The plasmid was transformed in *Escherichia coli* BL21 (DE3) strain. Transformed cells were grown at 293 K in Luria Broth medium, containing kanamycin resistance and 1.5 mM of the heme precursor δ-aminolevulinic acid (δ-ALA) to support the heme incorporation in *E. coli*, and incubated for about 70 hours. Given that the constitutive expression of the *E. coli* strain was sufficient to produce suitable amount of protein (~ 40 mg per litre of culture), induction with isopropyl β-thiogalactopyranoside (IPTG) has been avoided. After centrifugation, the harvested pellet was resuspended in 50 mM Tris·HCl and 300 mM NaCl, pH 8.0 and lysed by addition of a mixture of deoxyribonuclease, ribonuclease, lysozyme (Sigma Aldrich, St. Louise, Missouri, USA), protease inhibitors (cOmplete, EDTA-free, Roche, Basel, Switzerland), followed by sonication. The soluble fraction of the lysate, containing OleP, was loaded onto a 5 ml Hi-Trap Chelating HP column (GE Healthcare, Buckinghamshire, UK) equilibrated with 50 mM Tris·HCl and 500 mM NaCl, pH 8.0. OleP elutes at 200 mM imidazole. In order to cleave the histidine-tag, the protein sample was incubated overnight (~ 16 hours) at 277 K with bovine thrombin (Sigma Aldrich, St. Louise, Missouri, USA). Following a reverse passage into 5 ml Hi-Trap Chelating HP column, buffer was exchanged with 20 mM Bis-Tris pH 6.0 and the sample loaded onto a MonoQ column (GE Healthcare). OleP was eluted around 0.1 M NaCl.

In order to check sample homogeneity and degree of monodispersion, protein solution was loaded into a BioFox 17/1200 SEC (Knauer -Berlin, Ge) gel permeation column, and eluted in isocratic

mode in 20 mM Tris · HCl, pH 8.0. In this condition OleP elutes as a hexamer, given a retention time corresponding to a species 6 times larger than expected monomeric OleP (41 kDa). The equilibrium between the OleP oligomers shifts almost completely to the monomeric form by adding 0.2 M NaCl to the buffer (Figure S1).

Quality and quantity of purified protein was evaluated by SDS-PAGE and UV/visible spectra. Purified OleP was concentrated to about 1 mM and stored in 20 mM Tris·HCl pH 8.0 and 200 mM NaCl buffer at 193 K.

Equilibrium Binding Analyses. OleP binding affinity to both clotrimazole (CTZ) and ketoconazole (KC) was determined at 298 K and 288 K by titration of the enzyme at a concentration of 0.2 μM with the two inhibitors, in a total volume of 800 μL of 50 mM Hepes and 200 mM NaCl, pH 7.5. Stock solutions of CTZ and KC (Sigma Aldrich, St. Louise, Missouri, USA) were prepared at concentrations of 10 mM and 20 mM respectively, by dissolving the P450 inhibitors in DMSO. The final ligand concentration covered a range from 0 to 10 μM for both inhibitors. The final percentage of DMSO was kept below 1%. The adsorption shift induced by inhibitor binding to the OleP Soret peak was probed by collecting UV/visible spectra, recorded between 200 and 800 nm, after each substrate addition. Binding of inhibitor was monitored by following the adsorption shift of the heme γ-Soret peak of OleP from 413 to 433 nm, caused by the coordination of the azole nitrogen to the heme iron. Dissociation constant (K_D) was estimated using the Kaleidagraph software package, by plotting the absorbance intensities at 413 and 433 nm against the inhibitor concentration. Since the K_D values of the azole drugs were not markedly higher then the OleP concentration used, data were fitted with the quadratic equation:

$$\Delta AUobs = \frac{\Delta AUmax}{2}\left([E_0] + [I_0] + K_D - \left(([E_0] + [I_0] + K_D)^2 - 4([E_0][I_0])\right)^{\frac{1}{2}}\right) \quad \text{(Equation 1)}$$

where ΔAU_{obs} is the absorbance difference, ΔAU_{max} is the maximum absorbance difference extrapolated to infinite inhibitor concentration, and $[E_0]$ and $[I_0]$ are the enzyme and the inhibitor analytical concentrations, respectively. Data were also globally fitted with the program Prism

(Graphpad, Figure 2).

Inhibitor Binding Kinetics. The time evolution of the OleP interaction with CTZ and KC was followed by monitoring the absorbance increase at 433 nm on a SX18-MV stopped-flow apparatus (Applied Photophysics, Leatherhead, UK) using symmetric mixing mode. OleP, at a final constant concentration of 2.5 μM, was mixed with CTZ and KC diluted to the desired final concentration, ranging from 2.5 to 20 μM. Measurements were carried out in 50 mM Hepes, 0.2 M NaCl and 1% DMSO, pH 7.5, at 288 K. Control experiments indicated that the presence of 1% DMSO had no significant effects on the kinetic traces. The kinetic curves correspond to the average of at least three experiments, and they were satisfactorily fitted by a single exponential function using both the software provided by Applied Photophysics and the Kaleidagraph software package to obtain the observed rate constant, k_{obs}.

The k_{obs} were plotted versus inhibitor concentration (Figure 3) and analysed using the Kaleidagraph software package, using Equation 2, which is valid under pseudo-first-order conditions:

$$k_{obs} = k_{on} * n + k_{off} \qquad \text{(Equation 2)}$$

where k_{on} is the association constant, n is the inhibitor concentration and k_{off} is the dissociation constant.

Sample Preparation and X-ray Data Collection. Crystallization of unliganded OleP and in complex with inhibitors was carried out using the hanging-drop vapour-diffusion methods at 293 K, and 19 mg/ml of the purified protein in 20 mM Tris · HCl and 200 mM NaCl, pH 8.0. Crystals were obtained for the ligand-free OleP and by co-crystallization of the CTZ-bound form, using saturating concentration of inhibitor (2 mM), but diffraction at high resolution was observed only for crystals of the CTZ-OleP complex, grown in 1.6 M Ammonium Sulphate, 0.1 M Hepes Sodium Salt pH 7.5, 2% (w/v) PEG 1000 ($AmSO_4$ Suite n° 83, Qiagen). 20% PEG 200 was used as cryoprotectant. Diffraction data of CTZ-OleP crystal were collected at 100 K at ELETTRA (Trieste, Italy), beamline 5.2R, XRD1, using PILATUS detector. Data was indexed, scaled and integrated using the XDS package.[15] A summary is shown in Table 1.

Crystals grown from ligand-free OleP displayed diffraction only at low resolution (8 Å or less) showing multiple lattices, and therefore were useless for structural determination.

Structure Determination and Refinement. The determination of the initial crystallographic phases was performed by molecular replacement using MolRep[16] from the CCP4 suite.[17] The OleP amino acid sequence was submitted to BLAST search algorithm, to identify in the PDB database the best model for Molecular Replacement. Given the 48% sequence identity, the coordinates of the homologous P450 MycG (PDB ID: 2Y46) have been used as search model. The residues of the starting molecular model were renumbered and renamed using Chainsaw.[17] Iterative manual and automated refinement of the structure was carried out using Refmac5 in CCP4.[18]

Manual adjustment was performed using COOT with the Fo-Fc map contoured at 1σ and the 2Fo-Fc map at 3σ. Waters were added into the Fo-Fc map, contoured at 3σ, using the *Find Waters* tool of COOT. 5% of reflections was excluded from refinement and used for the R_{free} calculation.[19] Secondary structure assignment was performed using the Kabsch and Sander algorithm, and the geometrical quality of final models was assessed using Procheck.[20] Ramachandran statistics indicate no outliers for the CLT-OleP structure. The first 13 N-terminal residues in CTZ-OleP are missing in the models due to insufficient electron density. Final crystallographic statistics are shown in Table 1**,** data extend to 2.65 Å resolution with I/σ of 2.1 in the last resolution shell (2.81-2.65 Å). All figures were produced with PyMOL (http://pymol. sourceforge.net). The atomic coordinates and structure factors for CTZ-OleP structure have been deposited in the RCSB Protein Data Bank (accession codes 4XE3).

Results

Characterization of the azole binding mechanism

In order to assess the binding properties of OleP with azole compounds, two clinically used azole inhibitors, clotrimazole (CTZ) and ketoconazole (KC), differing for the N1-substituent group shape and chemistry, have been selected (Figure 1B).

Upon binding to the two azole compounds, OleP exhibits the typical *type II* spectral difference classically observed for previously characterized cytochrome P450s[21,22], with a peak at 433 nm and trough at 413 nm (Figure 2). The equilibrium binding transition of OleP to both CTZ and KC is consistent with a simple hyperbolic trend, returning apparent K_D values that we estimate to be in the nanomolar range for both inhibitors (K_D = 70 ± 6 nM for CTZ and K_D = 5 ± 1 nM for KC), with KC showing higher affinity by one order of magnitude, at pH 7.5 in the presence of 0.2 M NaCl at 298 K (Figure 2).

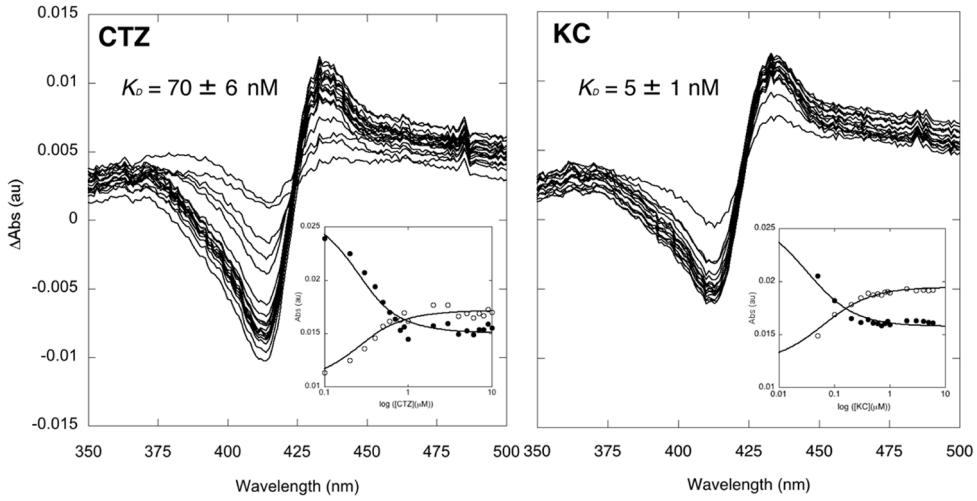

Figure 2. Equilibrium binding titration of OleP with clotrimazole (CTZ) and ketoconazole (KC). Difference spectral changes observed upon inhibitor binding are reported. Both CTZ (left panel) and KC (right panel) induce on OleP the typical *type II* spectral shift of the Soret peak that occurs upon azole binding to P450s, with a peak at 433 nm and a trough at 413 nm.

Insets report the absorbance changes at 413 (full dots) and 433 nm (empty dots) as a function of inhibitor concentration on a logarithmic scale, showing that the binding process involves a single event for both inhibitors. Protein has been used at a constant concentration of 0.3 μM at 298 K in 50 mM Hepes, pH 7.5. Data were fitted to Equation 1 (fits are shown as solid lines) to determine the dissociation constants, K_D, also reported.

In order to assess the binding mechanism of OleP to both CTZ and KC we followed the binding kinetics of OleP to both inhibitors at 288 K (at 298K the reaction was too fast for full detection, data not shown) and association (k_{on}) and dissociation (k_{off}) rate constants were determined by using a stopped-flow apparatus. *Quasi*-pseudo-first-order binding experiments were performed by mixing a constant concentration of OleP (2.5 μM) with increasing concentration of CTZ and KC, ranging from 2.5 to 20 μM. Under all conditions, the kinetics of formation of the complex with the inhibitor was fitted by a mono-exponential function, indicating a one-step mechanism, without evidence for the accumulation of detectable intermediate (Figure 3, Inset).

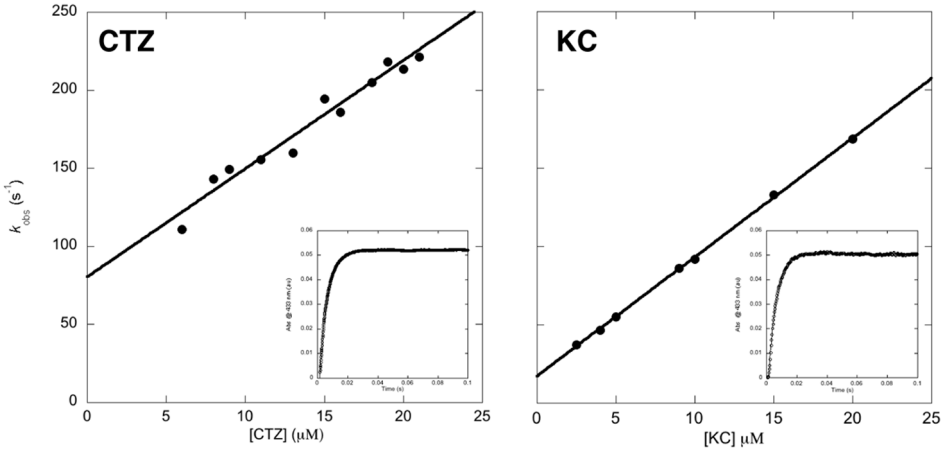

Figure 3. Pseudo–first-order kinetics of the binding between OleP and clotrimazole (CTZ) and ketoconazole (KC). Observed rate constants (k_{obs}, filled circles) are plotted as a function of [CTZ] and [KC]. The rate constants observed increase linearly with inhibitor concentration in both cases. Data were recorded at a concentration of 2.5 μM of OleP, mixed with variable concentrations of CTZ and KC, typically ranging between 2,5 and 20 μM, in 50 mM Hepes, 0.2 M NaCl and 1% DMSO at pH 7.5 and 288 K. Observed time courses were consistent with single-exponential behaviour in all cases. Inset reports the traces as the averages of three independent acquisitions obtained at 20 μM of inhibitors. Thin lines are the fit to a single exponential equation.

The linear dependence of the observed rate constants on CTZ and KC concentration confirmed the bimolecular nature of the two reactions. Data analysis yielded for CTZ an association bimolecular rate constant k_{on} = (6.9 ± 0.5) *10^6 $M^{-1}s^{-1}$ and an apparent dissociation rate constant $^{app}k_{off}$ = 80.4 ± 7.4 s^{-1} while for KC an association bimolecular rate constant k_{on} = (7.50 ± 0.08) *10^6 $M^{-1}s^{-1}$ and an apparent dissociation rate constant $^{app}k_{off}$ = 17.0 ± 0.9 s^{-1}.

The very high affinity of the two inhibitors towards OleP would require the accumulation of a number of points at nanomolar ligand concentrations. This would imply significantly decreasing protein concentration itself in order to maintain the pseudo-first order condition, at the expenses of the signal-to-noise ratio. The lack of points at low inhibitor concentration affects heavily the extrapolation of the off-rate constant, k_{off}, as obtained from data analysis shown in Figure 3, yielding values for K_D inconsistent with the same parameter measured directly by binding equilibrium at 288 K (K_D = 30 ± 15 nM for CTZ and K_D = 3.0 ± 0.6 nM for KC, data not shown). The simple one-step mechanism observed for both the formation of the OleP-inhibitor complexes allows a direct determination of the k_{off} by combining the association rate constants from binding kinetics with the affinity constants obtained by equilibrium experiments, yielding k_{off} = 0.21 ± 0.12 s^{-1} for CTZ and k_{off} = 0.022 ± 0.005 s^{-1} for KC.

OleP-CTZ: overall three-dimensional structure

In order to investigate the structure of OleP in the absence and in the presence of the two inhibitors, we attempted to crystallize both the ligand-free OleP and the CTZ and KC complexes. Nevertheless, only the CTZ-bound form yielded crystals that allowed structure determination. Crystals, diffracting to 2.65 Å, were grown by co-crystallization using saturating concentration of inhibitor (See Materials and Methods). Refinement of the CTZ-OleP model gave R_{factor}= 20.7 % and R_{free}= 26.0 % (Table 1).

Table 1. Data Collection, Refinements, Statistics and Validation for M86A-ErB structure

Highest-resolution shell is shown in parentheses.

Data Collection	
Resolution (Å)	50-2.65 (2.81-2.65)
Total measurements	238834
Unique reflections	34700
Completeness (%)	99.1 (95.4)
Redundancy	6.88 (5.87)
R_{merge}[a] (%)	9.0 (86.0)
I/σ (I)	17.3 (2.1)
Wilson B-value ($Å^2$)	54.3
Refinement	
Resolution (Å)	48.76-2.65 (2.81-2.65)
Reflections	32972
Molecules per asymmetric unit	2
Space group	$C222_1$
Unit cell (Å, °)	a = 115.94, b = 117.38, c = 174.66
R_{work} /R_{free}[b] (%)	20.7/26.0
Mean B-factors ($Å^2$)	
Protein (Chain A/ChainB)	59.3/58.4
Heme (Chain A/Chain B)	4.3/5.2
Ligand, CTZ (Chain A/Chain B)	7.9/9.9
Water/Sulphate	44.4/65.5
Deviation from ideal geometry	
Bond (Å)	0.011
Angles (°)	1.77
Ramachandran (%) Favoured/allowed/outliers*	93.6/6.4/0.0
No. of atoms	
Protein	6156
Heme/Ligand	86/50
Water	57
Sulphate	50
Solvent content (%)	62.6

[a] $R_{merge} = \sum_i \sum_j \left| I_{I,j} - \langle I_j \rangle \right| / \sum_i \sum_j I_{i,j}$, where *i* runs over multiple observations of the same intensity, and *j* runs over all crystallographically unique intensities.

[b] $R_{work} = \sum \left| |F_{obs}| - |F_{calc}| \right| / \sum |F_{obs}|$, where $|F_{obs}|>0$. R_{free} is based on 5% of the data randomly selected and is not used in the refinement.

*No Prolines and Glycines.

The CTZ-bound form is organized as a dimer in the asymmetric unit, the two monomers are held

together by electrostatic interactions mediated by water molecules and sulphate ions (Figure 4A). Following the standard nomenclature for P450 structures [23], the two monomers are spatially arranged in a back-to-back conformation, rotated by 180° (Figure 4A).

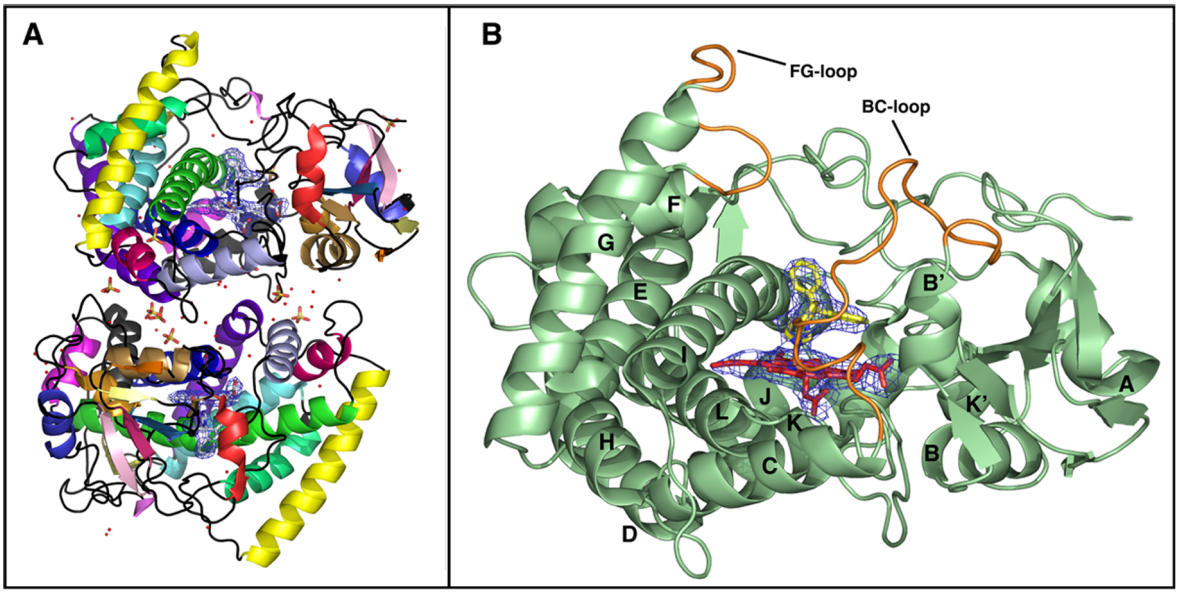

Figure 4. OleP-CTZ: overall structure. A. Cartoon representation of the two monomers found in the asymmetric unit. Molecules of water and sulphate ions are also shown, respectively as red dots and stick model. Most of them are placed at the interphase between dimers. Secondary structural elements are represented using different colours to highlight the mutual orientation of the two monomers. **B.** CTZ (light yellow sticks) bound to OleP structure (light green ribbon) is displayed, as observed in monomer A. OleP is here represented in a non standard P450 orientation to allow a clear visualization of the inhibitor bound to the active site. Capital letters indicate the secondary structure elements according to P450 nomenclature. BC-loop and FG-loop are labelled and coloured in orange. In both panels the electron density map contoured at 1σ around the heme group (red sticks) and CTZ is also shown.

The superposition of the structural elements reveals the overall conformation of the two monomers to be roughly the same, with the exception of slight movements (< 2.5 Å) of residues 170-194 (helix

F, FG loop and the N-term of helix G) and of residues 394 and 395 at the C-term (overall rmsd mean of the C_α carbons 0.56 Å for the whole structure).

In order to assess the functional significance of the dimer, we performed gel filtration analysis to determine the oligomerization state of OleP in solution under physiological conditions. At low ionic strength conditions (50 mM Tris · HCl, i.s.= 0.028 M) OleP assumes predominantly a hexameric form, possibly induced by intermolecular electrostatic interactions. We subsequently observed that OleP shifts almost completely to a monomeric state at higher ionic strength, with values considered corresponding to the intracellular environment (0.2 M NaCl, i.s.= 0.2 M) (Figure S1). Moreover, equilibrium binding experiments performed at 0.2 M NaCl on KC and CTZ yield saturation curves which fit to single hyperbolic equation, thus accounting for a single binding event without detectable cooperativity.

The overall structure and protein topology of OleP correspond to those of other P450 enzymes. The secondary structural elements of OleP consist of 15 helices and two β-sheet spatially arranged in the typical prism-like fold of cytochrome P450s (Figure 4B). The enzyme internal cavity, containing the prosthetic group, is 590 $Å^3$ in volume. As previously observed for other P450s, the heme group is buried at the bottom of the active site and located between the internal helix I and the proximal helix L. A salt bridge with Arg298 and a hydrogen bond with His101 are established by the two tetra-porphyrin propionates, anchoring the heme group bound to the protein matrix (Figure 5A-B). As a hallmark for P450s, the thiolate group of cysteine 356 in OleP coordinates the heme iron in the fifth position, while the water molecule that in the resting-state of the enzyme occupies the sixth one, is, in this structure, replaced by a molecule of CTZ (Figure 5A-B).

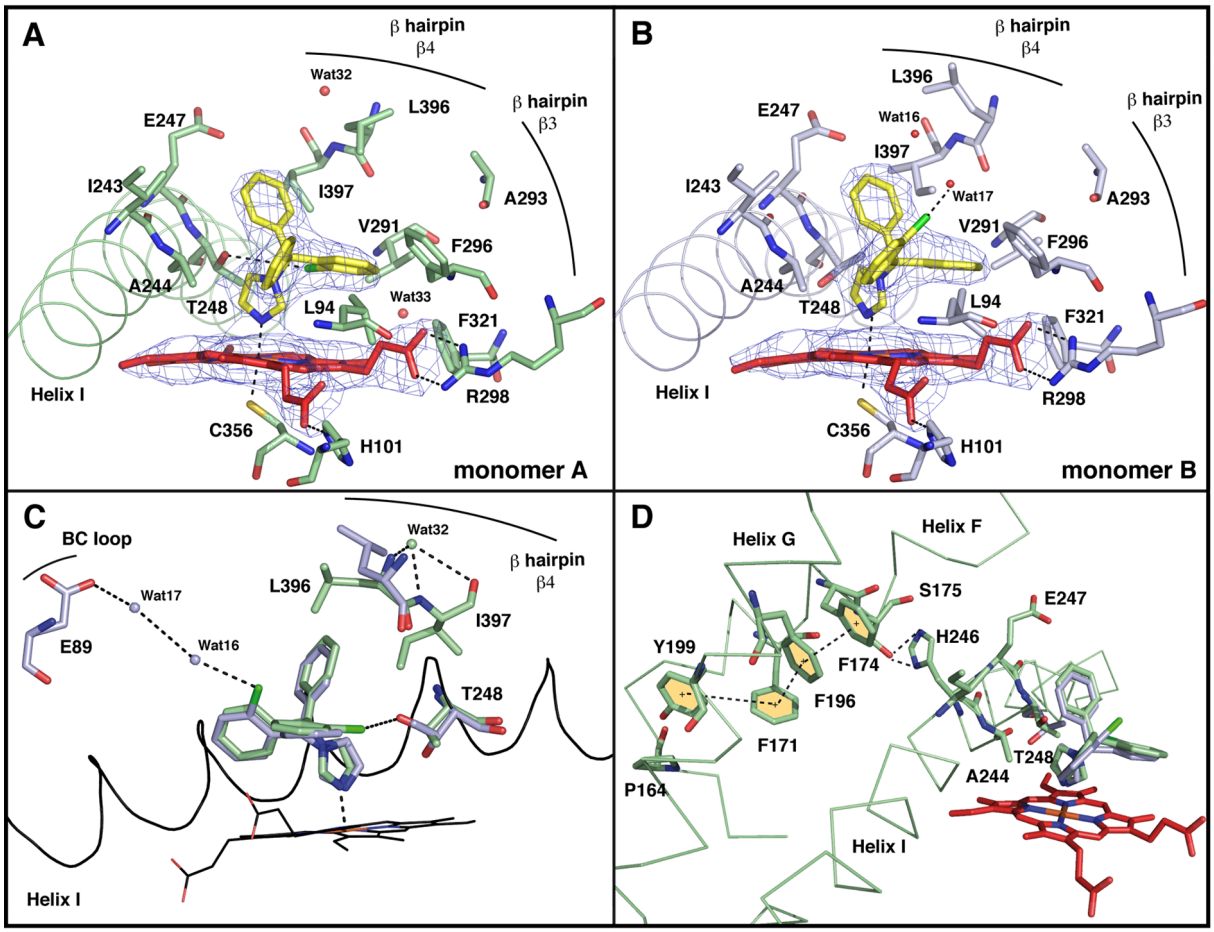

Figure 5. CTZ in the active site of OleP. A-B. OleP residues interacting with CTZ and located within 4.5 Å of the inhibitor are represented as found in both orientations assumed by the N1-substituent group of CTZ in the two monomers (respectively, monomer A, panel A and monomer B, panel B). Electron density omit map (2Fo-Fc) contoured at 1.0 σ around CTZ and the heme group is also shown. Aminoacids (light green for monomer A, light blue for monomer B), heme group (red) and the CTZ molecule (yellow) are represented as stick and water molecules as red spheres. Dashed lines indicate coordination bonds and halogen-hydrogen bonds in both panels. **C. Effect of the alternative conformations of the CTZ N1-substituent group on the organization of the active site residues and on water molecules.** The rotation of 120° clockwise around the chemical bond between N1 and the side chain of CTZ is accommodated into OleP active site by forming in both cases a halogen-hydrogen bond with the chloride substituent of the phenyl ring of CTZ. In monomer A (light green stick) the halogen-hydrogen interaction directly involves the

hydroxyl group of the conserved Thr248 on helix I. In monomer B (light blue stick representation) a water molecule (Wat16) becomes the partner of the halogen-hydrogen interaction. Wat16 interacts *via* Wat17 with Glu89 on the BC-loop. The alternative conformations assumed by Thr248 and Leu396 are also highlighted. Helix I and heme group are in black, respectively shown as ribbon and stick representation. Water molecules are labelled and represented as spheres coloured by following the relative monomer structure. Dashed lines indicate coordination bonds, hydrogen and halogen-hydrogen bonds. **D. The pi-stacking chain in OleP.** The "π-π zipper" is shown. Hydrogen bonds and pi-stacking interactions (distance < 4.3 Å) are represented using dashed lines. Residues involved in the network (light green), CTZ (light green, monomer A; light blue monomer B) and heme group are represented as stick. The secondary structural elements involved in the network are labelled and reported in ribbon representation (light green).

CTZ bound to OleP: Active site overview and analysis of the surrounding secondary structural elements

The initial electron density omit maps, calculated without the azole inhibitor, revealed clear electron density in the active site corresponding to a molecule of CTZ (Figure 5A-B). The N3 of the imidazole moiety of CTZ coordinates in the sixth position the heme iron at a distance of 1.96 Å in monomer A and 2.09 Å in monomer B, azole coordination being visible as continuous electron density.

The three aromatic rings, two phenyl- and a chlorophenyl- moieties, that compose the bulky side chain of CTZ, are mainly involved in van der Waals interactions with residues lining the active site and located on the BC-loop (Leu94), the β-hairpins β_3 (Val291, Ala293, Phe296, Arg298), helix I (Ile243, Ala244, Glu247, Thr248), helix K' (Phe321) and the β-hairpin β_4 (Leu396 and Ile397) (Figure 5A-B). Notably, all the residues involved in interactions with CTZ are placed in segments of the polypeptide chain corresponding to regions typically involved in Substrate Recognition Segments in P450s (SRS1, BC loop; SRS4, helix I; SRS5 and 6 the β-hairpins β_3 and β_4).[24]

The CTZ molecule assumes different orientations in monomer A and B (Figure 5A-B), which we could assign upon examination of the electron density omit maps. The chloride atoms in the chlorophenyl moiety guided us in identifying two positions for the side chain of CTZ, rotated clockwise by 120° around the bond with N1 in azole moiety (Figure 5C). In both the orientations a halogen-hydrogen interaction involves the chloride substituent of the phenyl ring of CTZ. In monomer A the halogen-hydrogen bond is directly formed with the hydroxyl group of the conserved Thr248 on helix I (Figure 5C). Conversely, in monomer B a water molecule (Wat16) becomes the partner of the halogen-hydrogen interaction. Wat16 interacts *via* Wat17 with Glu89 on the BC loop, moreover the side-chain of Thr248 rotates pointing its –OH group towards the heme. Notably, comparing the two monomers, Thr248 and Leu396 are the sole residues of the active site that were found in alternative conformations (Figure 5C).

Hence, the absence of fully specific interactions, which would constrain the CZT side chain to a unique conformation, provides enough freedom to allow rotation around the pivot-like imidazole moiety that is held by the coordination bond with the heme iron.

In spite of the different orientations of CTZ in its active site, OleP adopts a unique arrangement of its secondary and tertiary structures. Moreover, given the failure in obtaining ordered crystals with unliganded OleP, we hypothesize that the presence of CTZ bound to the heme reduces the structural dynamics of OleP, introducing enough rigidity to allow crystallization. Analysing the structure we observed that OleP bound to CTZ assumes an open conformation, with the active site largely exposed to the solvent, the minimum distance between the BC-loop and the FG-loop being about 10.5 Å. In other P450s, the structural primer that triggers the conformational response to ligand binding is the long helix I that arches over the heme crossing the entire active site and that directly interacts with bound ligands.[25] A closer look indicates that the closest contact of CTZ in the binding site, where the coordination bond to the heme iron acts as a tight constraint, is indeed with the central residues of the helix I, namely Ile243, Ala244, Glu247 and Thr248. The bound imidazole introduces a local point hindrance mainly on Ala244 and Thr248 (Figure 5D) inducing a minor

distortion of one turn of helix I that determines the "collapse" of the catalytic cleft, as previously reported for other P450-azole complex structures. [25-27]

We searched for specific interactions stabilized by the presence of CTZ in the active site that could limit the flexibility of the OleP fold. The only candidate appears to be His246, flanked by the residues of helix I in closest contact with the imidazole moiety, which forms two H-bonds with Ser175 on helix F. This interaction connects helix I to a π-π stacking chain between helices F and G shown in Figure 5D that involves Phe174, Phe171, Phe196 and Tyr199. Such cluster of pi-stacking interactions forms a "zipper" that holds together helices F and G and the FG loop, resulting in a unique structural block, with Pro164 on the EF loop closing the chain (Figure 5D).

This long-range network that connects the internal cavity (helix I) with the outer areas of the enzyme (helixes F and G), bolstered by such a cluster of π-π interactions [28,29] fastens in a precise layout the portion of the structure that spans from helix I to helixes F and G including the FG loop.[30]

Comparison with other macrolide epoxigenases

OleP represents the fifth macrolide epoxigenases from actinomycete organism that has been structurally characterized. The closest structural homologous (48% of identity, Figure S2) is the P450 MycG (Dali Database[31]), whose coordinates have been used as molecular replacement model for OleP (See Materials and Methods, PDB ID: 2Y46).

MycG is a multifunctional monooxygenase from *M. griseorubida* involved in mycinamicin biosynthesis.[12] It performs sequential reactions of hydroxylation and epoxidation on two sites, a tertiary allylic C-H bond and an olefin, of two metabolic intermediates of the mycinamicin pathway, respectively mycinamicin IV (M-IV) and V (M-V) (Figure 1C,[12]). Both M-IV and M-V are considerably different from the OleP proposed substrates, 8.8a-oleandolyde (DEO) and the monoglycosylated L-olyvosil-8.8a-deoxyoleandolide (LO-DEO, Figure 1A), being doubly glycosylated, with the two sugar moieties attached on the opposite sides of the macrolactone ring.[12]

In spite of the diversities of the substrates and of the three times larger cavity volume of MycG, the

overall structures of the two P450s are very similar, with an overall rmsd for C_α of 1.5 ± 0.7 Å. Only five regions display a C_α rmsd exceeding 4 Å: 44-51, 73-93, 133-142, 178-196, and 302-314, some of these segments are involved in substrate recognition and/or others are externally exposed (Figure S2).

Given the structural similarity and taking advantage of the body of information available in the literature, MycG represents the best model of epoxigenase to compare with OleP and it could provide some insight on its specific features linked to substrate binding and catalysis.

Indeed, several MycG structures have been determined both in its ligand-free form and in complex with the two physiological substrates, M-IV and M-V, and with the biosynthetic precursor mycinamicin III (M-III). Structural analysis of the unproductive complex with M-III revealed that the substrate can adopt two binding modes, one orthogonal and the other parallel to the heme. Nevertheless, given the distance between the catalytic centre of the enzyme and the targeted mycinamicin carbons, it has been proposed that in MycG the orthogonal binding mode of substrates is an “en route” configuration, on the way to the catalytically competent parallel orientation.[12]

Sequence alignment and structural superposition to the CTZ-OleP structure revealed that several active site residues critical for both the parallel and the orthogonal M-III binding in MycG are conserved in OleP and involved in contacts with CTZ (Figure 6).

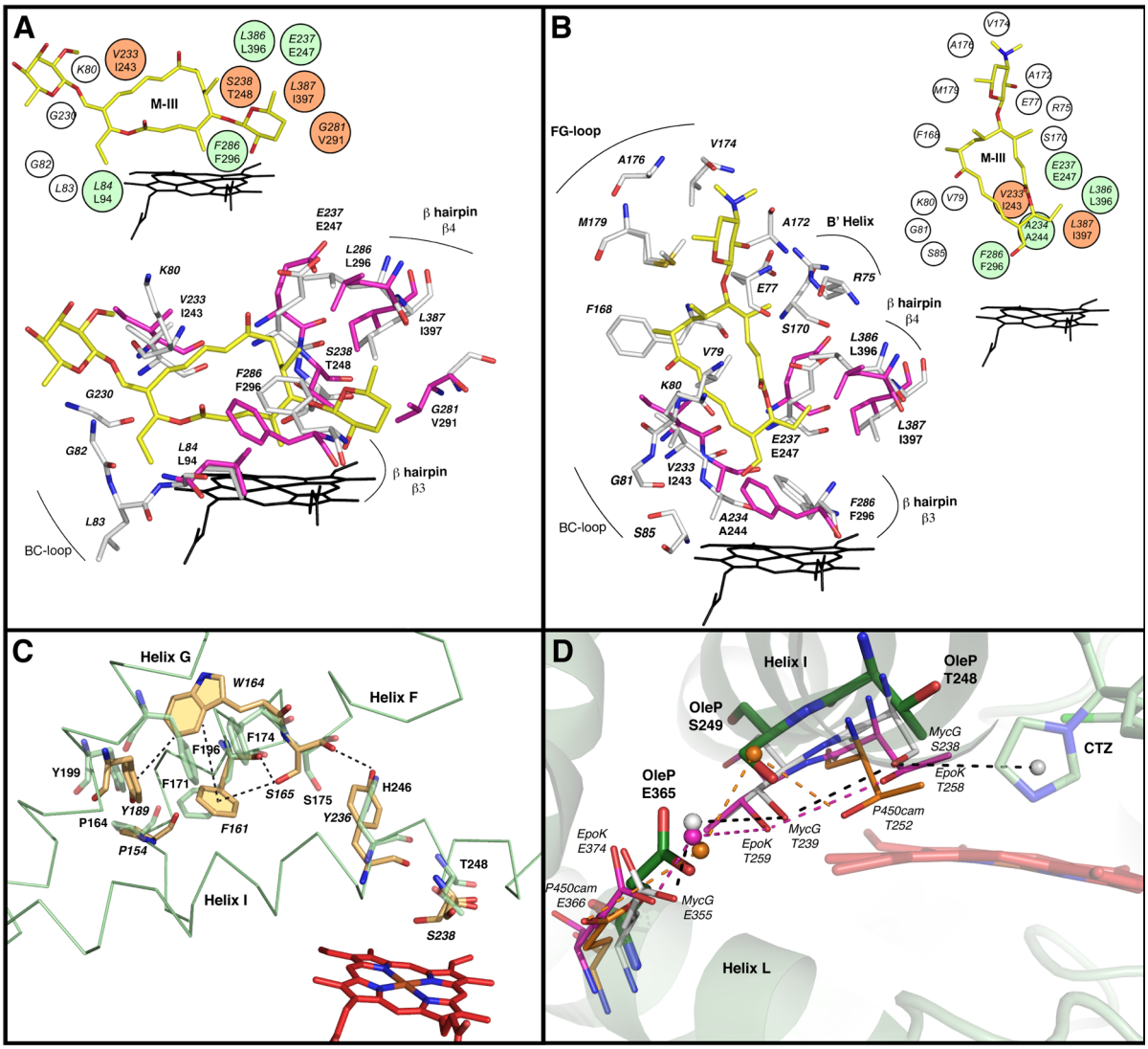

Figure 6. Comparison with MycG and other P450 epoxigenases. A-B. OleP residues involved in CTZ interaction (pink stick) are shown and superposed to the residues in the active site of MycG (white stick) that interact with M-III (yellow stick) both in the parallel (Panel A) and in the orthogonal (Panel B) binding mode. A schematic representation of the superposed active site of MycG and OleP is also reported at the top of the panels, showing residues as spheres differing in size and colour: small-white spheres represent residues not conserved, big-orange represent strongly similar residues, and big-green spheres indicate the conserved residues. Residues are labelled using italic font for MycG. **C. The pi-stacking network.** The superposition of the pi-network of CTZ-OleP (light green) and MycG (light orange, PDB ID: 2Y46) is shown. Residues involved in the chain and the heme group (red) are given in stick. Italic font is used to label the MycG residues.

Dashed lines indicate the π-stacking interactions (distance < 4.7 Å). Capital letters indicate the secondary structure elements (reported in ribbon representation) according to P450 nomenclature. **D. The proposed proton shuttle pathway in OleP.** Superposition of CTZ-OleP structure (green) and M-IV-MycG (white, PDB ID: 2Y46[12]), EpoD-EpoK (pink, PDB ID: 1PKF[13]) and P450cam (orange, PDB ID: 3L63[47]) structures highlighting the water molecule chain involved in protons delivery during the catalytic reaction. No water molecules were found in CTZ-OleP given the CTZ induced disruption of the helical cleft. Heme groups (red), CTZ (green) and side chains are in stick. Black, pink and orange broken lines indicate H-bonds respectively in M-IV-MycG, EpoD-EpoK and P450cam. Water molecules are labelled and represented as spheres, coloured following the corresponding structure.

Panel A of Figure 6 shows the parallel substrate binding mode observed in MycG, superimposed to the OleP active site, highlighting the residues involved in binding (MycG) and the corresponding ones in OleP. From this comparison we conclude that this binding mode is fully compatible with the structure of the site in OleP.

Since both potential OleP substrates lack the sugar in C5 (desosamine), the macrolide ring could shift towards Val291, bringing the target C-C bond at optimal reaction distance with the heme iron. Moreover further analysis of the active site shows that no steric clash for the olivosyl moiety on C3 of LO-DEO is present in OleP. Therefore, both LO-DEO and DEO could productively bind OleP in a parallel binding mode.

As far as the “en route” orthogonal binding mode observed in MycG is concerned (Panel B of Figure 6), we conclude that the OleP glycosylated substrate, LO-DEO, cannot productively bind in this orientation since the target carbons are on the same side of the macrolactone ring with respect to the sugar (Figure 1A).

Another common feature of the two macrolide-epoxigenases is the network of pi-stacking interactions that holds together helices F and G and the FG loop. In MycG this network involves

Ser238 and Tyr236 on helix I, Ser165, Trp164 and Phe161 on helix F, Tyr189 on helix G and Pro154 on the EF loop, with the parallel stacking of the two Phe in OleP replaced by a tryptophan in MycG (Figure 6C). In the same region, other P450 epoxigenases, AurH, PimD and EpoK, are rich of hydrophobic aliphatic residues that interact weakly, allowing helices F and G to slide with respect to each other, facilitating the closure of the structure upon their substrates.[11,14,32] Conversely, in OleP and MycG we find a pi-stacking network that reduces flexibility in the F-G segment thus preventing relative displacements of helices F and G and of the loop in between. Indeed in MycG, no major conformational rearrangements have been observed between unbound and bound structures. Nevertheless, we cannot exclude for OleP the possibility to explore alternative conformations upon substrate binding, that in P450 have a canonical feature in the lid-like motion of the BC and FG-loops.[33-35] In CTZ-OleP these loops are 10.5 Å apart, suggesting that CTZ does not trigger closure of the binding site or that OleP can not achieve a "closed" structure. The largest difference in sequence between OleP and MycG falls in the protein segment that comprises the helix B' and the BC loop (Figure S2). The sequence differences within this region could account for the evolutionary divergence undergone by the two P450s for achieving their substrate specificities and, possibly, binding mechanisms. As a matter of fact, this region, typically involved in substrate recognition, is also often responsible for the conformational movements of the protein occurring upon ligand or substrate binding.

Multiple sequence alignment and structural comparison with the two epoxigenases MycG and EpoK indicate the residues that are likely to be involved in the water chain responsible for the P450 proton delivery during the catalytic cycle.[12,32] This network generally starts with a conserved threonine on helix I, located into the active site, and ends with a glutamate placed on the solvent-exposed helix L.[36] In OleP we assign Thr248 as the direct proton donor to the catalytic peroxy-intermediate and Glu365 as the final residue of the chain, with Ser249 connecting them (Figure 6D). As previously observed for other P450s, the presence of an inhibitor in the active site and the consequent disruption of the catalytic cleft on helix I prevent the incorporation of the *quasi-*

structural water molecules that bridge this catalytic chain and that should be placed inside the groove between Ser249 and Glu365, as expected by comparison with the substrate-bound structure of P450cam, EpoK and MycG (Figure 6D).

Discussion

Unravelling the molecular determinants of the dualism between specificity and versatility represents a conundrum for research on P450s. Dissecting the structure-function relationship of individual forms of P450 allows to understand how different and fine-tuned functionalities are achieved by changing a limited set of key-residues, thus providing inspiration for protein engineering.[4,37,38] Moreover, the universal phylogenetic distribution of the members of this family and their involvement in many different metabolic pathways provide the opportunity to exploit P450s as alternative drug targets for antimicrobial therapy as well as in treatment of metabolic disorders and cancer.[39-42] However, in order to achieve the required specificity to avoid or at least limit drug side effects, structural and functional information on individual P450s are required.

In this context, we report the crystal structure of the bacterial cytochrome P450 epoxigenase OleP, obtained in complex with a common P450 inhibitor, clotrimazole (CTZ), and the characterization of the OleP binding mechanism to CTZ and to another azole, ketoconazole (KC), of different molecular size and nature.

In complex with the bulky molecule of CTZ, OleP crystallizes as a dimer, with both monomers arranged in an open conformation. The main driving force for CTZ binding is the coordination between the azole moiety and the heme iron of OleP, as also confirmed by kinetic measurements. Nonetheless, the hydrophobic interactions that the side chain of CTZ establishes into the internal cavity of the enzyme provide a rational for the stabilization of an open conformation induced by the inhibitor. As expected, many of these interactions involve regions of the protein that are generally described as critical for substrate binding and recognition in P450s. But additionally, we found that most of the interacting residues are conserved and involved in substrate binding in the closest homologue of OleP, the P450 epoxidase MycG. This finding supports the idea that those residues

are also involved in the recognition of the two possible substrates of OleP, 8.8a-deoxyoleandolide (DEO) and L-olivosyl-8.8a-deoxyoleandolide (LO-DEO). By comparison with the complexes of MycG with its substrates, we suggest alternative binding modes also for OleP and its two putative molecular targets.

Although the absence of substrate-bound structures of OleP limits our view of this system, the rigidity conferred by the pi-stacking chain that fastens the FG-portion suggests that structural changes undergone by OleP to achieve a "closed" conformation would mostly involve the flexible BC and FG-loop regions. We speculate that, in the presence of a physiological ligand, the BC-loop of OleP would establish specific contacts, allowing the closed conformation necessary for catalysis.

Stopped-flow kinetic measurements provided further information on the OleP binding mechanism. For CTZ and KC inhibitors the reaction behaves as a simple one-step process, with no detectable intermediates. The binding event is mostly driven by the formation of the coordination bond between the imidazole moiety and the heme iron, that represents the rate-limiting step of the reaction, as accounted by the comparable k_{on} values observed for CTZ and KC. The higher affinity of OleP towards KC with respect to CTZ results from the dissociation rate constants (k_{off}), since CTZ and KC differ for the N1-substituent group, the k_{off} values are likely affected by the interactions within the binding site as well as by the conformational response induced in OleP.

We propose that the simple A+B $\rightarrow$ AB binding mechanism observed for CTZ occurs *via* the coordination to the heme of a dynamic open form of OleP that is stabilized by the interaction with the inhibitor, as observed in the crystal structure. Moreover, binding of CTZ would lock OleP in a stable open form, allowing crystallization, at variance with the unliganded and KC-bound enzyme. We deduced that KC induces a structural transition that hinders ligand dissociation from the one order of magnitude lower k_{off} value observed with respect to the CTZ-OleP complex that crystallizes in an open conformation. The spectral transitions upon CTZ and KC binding provide another clue, beyond the resilience to crystallization, of the structural heterogeneity of the KC-OleP complex. Indeed, CTZ induces a spectral transition twice larger than the one observed upon KC

binding (Figure 2 and Figure S3). The *type II* spectral shift of P450s upon azole binding is due to a stabilization of the low-spin state[43], more pronounced if the ligand is limited in its mobility.[44] Given these considerations we hypothesize that KC induces the shift of OleP to a population of states with reduced active site accessibility (lower k_{off}), higher ligand mobility (reduced spectral shift) and no propensity to crystallization, in spite of the higher overall ligand affinity.

Concluding Remarks

In organic synthesis, epoxides are versatile building blocks, often used as intermediates to add functional groups to olefinic or aromatic substrates.[45] Remarkably, very few chemical processes allow for direct epoxidation of aliphatic C-H or C-C bonds and most of these synthetic methods are either not selective or are inefficient, especially on large substrates containing multiple reactive centres. Given their exceptional chemical reactivity and biodiversity, macrolide-P450 epoxigenases are considered a powerful system to be exploited to introduce epoxide functions in order to generate innovative polyketide derivatives and alternative pharmaceutical products in industrial semi-synthetic preparation.[4]

In this context, the chemistry carried out by OleP is intrinsically interesting and very rare. Among the structurally known macrolide-epoxigenases, OleP is the only one that introduces an epoxide function on a non-activated C-C bond. It has been proposed that OleP might carry out this reaction *via* an olefinic intermediate, but the mechanism is still unknown.[7]

Moreover, the structure of a novel P450 in complex with an azole inhibitor adds rational tools to design selective inhibitors against homologue P450s involved in essential metabolic pathways of pathogenic organism, such as CYP141, which has been proposed as novel therapeutic target against *Mycobacterium tuberculosis*[46], that shares almost the 35% of sequence identity with OleP.

In conclusion, the structural-functional data here presented represent a starting point to understand the interesting and rare chemistry carried out by OleP, aiming at engineering the enzyme to redirect its specific physiological function into alternative desired reactions, and to design more selective and potent anti-P450 drugs for antimicrobial therapy.

Acknowledgments

We thank Biotica Technology, Ltd., UK and Steven G. Kendrew for the kind gift of the plasmid pSGOleP, a pUC18 cloning vector containing the nucleotide sequence coding for OleP. The crystallographic experiments were performed on the 5.2R, XRD1 beamline at the ELETTRA Synchrotron, Trieste, Italy. We are grateful to Maurizio Polentarutti at the ELETTRA (Trieste, Italy), for providing assistance in using beamline 5.2R. The research leading to these results has received funding from the European Community's Seventh Framework Programme (FP7/2007-2013) under grant agreement nº 283570.

References

1. Coon, M. C. (2005) CYTOCHROME P450: Nature's Most Versatile Biological Catalyst, *Annu. Rev. Pharmacol. Toxicol. 45*, 1–25. doi:10.1146/annurev.pharmtox.45.120403.100030
2. Nelson, D. N., and Strobe, H. W. (1987) Evolution of Cytochrome P-450 proteins, *Mol. Biol. Evol. 4*(6), 572-593. 0737-4038/87/0406-0002$02.00
3. Denisov, I. G., Makris, T. M., Sligar, S. G., and Schilichting, I. (2005) Structure and chemistry of cytochrome P450, *Chem. Rev. 105*, 2253–2277. doi: 10.1021/cr0307143.
4. Grogan, G. (2011) Cytochromes P450: Exploiting diversity and enabling application as biocatalysts, *Curr. Opin. Chem. Biol. 15(2),* 241-248. doi: 10.1016/j.cbpa.2010.11.014.
5. Rabe, K. S., Gandubert, V. J., Spengler, M., and Niemeyer, C. M. (2008) Engineering and assaying of cytochrome P450 biocatalysts, *Anal Bioanal Chem. 392*, 1059–1073. doi: 10.1007/s00216-008-2248-9.
6. Quiros, L., and Salas, J. (1995) Biosynthesis of the Macrolide Oleandomycin by Streptomyces antibioticus. Purification and kinetic characterization of an Oleanomycin Glucosyltransferase, *J Biol Chem. 270*, 18234–18239. doi: 10.1074/jbc.270.31.18234.

7. Gaisser, S., Lill, R., Staunton, J., Méndez, C., Salas, J., and Leadlay, P. F. (2002) Parallel pathways for oxidation of 14-membered polyketide macrolactones in Saccharopolyspora erythraea, *Mol. Microbiol. 44*, 771–781. doi: 10.1046/j.1365-2958.2002.02910.x.
8. Rodriguez, A., Olano, C., Méndez, C., Hutchinson, C., and JA, S. (1995) A cytochrome P450-like gene possibly involved in oleandomycin biosynthesis by Streptomyces antibioticus, *FEMS Microbiol Lett. 127*, 117–120. doi: 10.1111/j.1574-6968.1995.tb07459.x.
9. Shah, S., Xue, Q., Tang, L., Carney R., J., Betlach, M., and McDaniel, R. (2000) Cloning, characterization and heterologous expression of a polyketide synthase and P-450 oxidase involved in the biosynthesis of the antibiotic oleandomycin, *J. Antibiot. 53(5)*, 502–508. doi: 10.7164/antibiotics.53.502.
10. Tatsuta, K., Gunji, H., Tajima, S., Ishiyama, T., Imai, S., Okuyama, S., and Fykatsu, S. (1990) Biosynthetic studies on oleandomycin by incorporation of the chemically synthesized aglycones, *J. Antibiot. 43*, 909–911. doi: 10.7164/antibiotics.43.909.
11. Kells, P., Ouellet, H., Santos-Aberturas, J., Aparicio, J., and Podust, L. (2010) Structure of cytochrome P450 PimD suggests epoxidation of the polyene macrolide pimaricin occurs via a hydroperoxoferric intermediate, *Chem. Biol. 17*, 841–851. doi: 10.1016/j.chembiol.2010.05.026.
12. Li, S., Tietz, D. R., Rutaganira, F. U., Kells, P. M., Anzai, Y., Kato, F., Pochapsky, T. C., Sherman, D. H., and Podust, L. M. (2012) Substrate recognition by the multifunctional cytochrome P450 MycG in mycinamicin hydroxylation and epoxidation reactions, *J. Biol. Chem. 287*, 37880–37890. doi: 10.1074/jbc.M112.410340.
13. Nagano, S., Li, H., Shimizu, H., Nishida, C., Ogura, H., Ortiz de Montellano, P., and Poulos, T. (2003) Crystal structures of epothilone D-bound, epothilone B-bound, and substrate-free forms of cytochrome P450epoK, *J. Biol. Chem. 278*, 44886–44893. doi: 10.1074/jbc.M308115200.

14. Zocher, G., Richter, M., Mueller, U., and Hertweck, C. (2011) Structural Fine-Tuning of a Multifunctional Cytochrome P450 Monooxygenase, *J. Am. Chem. Soc. 133*, 2292–2302. doi: 10.1021/ja110146z.

15. Kabsch, W. (2010) XDS, *Acta Crystallogr. D Biol. Crystallogr. 66*, 125–132. doi: 10.1021/ja110146z.

16. Vagin, A., and Teplyakov, A. (1998) A translation-function approach for heavy-atom location in macromolecular crystallography, *Acta Cryst. D54*, 400–402. doi: 10.1107/S0907444997014923.

17. Collaborative Computational Project, N. 4. (1994) The CCP4 suite: programs for protein crystallography. *Acta Cryst. D50*, 7690–7763. doi: 10.1107/S0907444994003112.

18. Pannu, N., Murshudov, G., Dodson, E., and Read, R. J. (1998) Incorporation of prior phase information strengthens maximum-likelihood structure refinement, *Acta Crystallogr., Sect. D 54*, 1285−1294. doi: 10.1107/S0907444998004119.

19. Brunger, A. T. (1992) Free R value: a novel statistical quantity for assessing the accuracy of crystal structures. *Nature 355*, 472–475. doi:10.1038/355472a0.

20. Laskowski, R., MacArthur, M., Moss, D., and Thornton, J. (1993) PROCHECK: a program to check the stereochemical quality of protein structures, *J. Appl. Cryst. 26*, 283–291. doi:10.1107/S0021889892009944.

21. Isin, E. M., and Guengerich, P. (2008) Substrate binding to cytochromes P450. *Anal. Bioanal. Chem. 392*, 1019–1030. doi: 10.1007/s00216-008-2244-0.

22. Zhang, W., Ramamoorthy, Y., Kilicarslan, T., Nolte, H., Tyndale, R. F., and Sellers, E. M. (2002) Inhibition of cytochromes P450 by antifungal imidazole derivatives, *Drug Metab. Dispos. 30*, 314–318. doi: 10.1124/dmd.30.3.314.

23. Haniu, M., Armes, L. G., Tanaka, M., Yasunobu, K. T., Shastry, B. S., Wagner, G. C., and Gunsalus, I. C. (1982) The primary structure of the monoxygenase cytochrome P450CAM, *Biochem. Biophys. Res. Commun. 105*, 889–894. doi:10.1016/0006-291X(82)91053-1.

24. Gotoh, O. (1992) Substrate recognition sites in cytochrome P450 family 2 (CYP2) proteins inferred from comparative analyses of amino acid and coding nucleotide sequences, *J. Biol. Chem. 267*, 83–90.

25. Montemiglio, L. C., Gianni, S., Vallone, B., and Savino, C. (2010) Azole drugs trap cytochrome P450 EryK in alternative conformational states, *Biochemistry 49*, 9199–9206. doi: 10.1021/bi101062v.

26. Cupp-Vickery, J. R., Garcia, C., Hofacre, A., and McGee-Estrada, K. (2001) Ketoconazole-induced conformational changes in the active site of cytochrome P450eryF, *J. Mol. Biol. 311*, 101–110. doi:10.1006/jmbi.2001.4803.

27. Ekroos, M., and Sjogren, T. (2006) Structural basis for ligand promiscuity in cytochrome P450 3A4, *Proc. Natl. Acad. Sci. 103*, 13682–13687. doi: 10.1073/pnas.0603236103.

28. Chelli, R., Gervasio, F., Procacci, P., and Schettino, V. (2002) Stacking and T-shape competition in aromatic-aromatic amino acid interactions, *J. Am. Chem. Soc. 124*, 6133–6143. doi: 10.1021/ja0121639.

29. McGaughey, G., Gagné, M., and Rappé, A. (1998) pi-Stacking interactions. Alive and well in proteins, *J. Biol. Chem. 273*, 15458–15463. doi: 10.1074/jbc.273.25.15458.

30. Cockroft, S., Hunter, C., Lawson, K., Perkins, J., and Urch, C. (2005) Electrostatic Control of Aromatic Stacking Interactions, *J. Am. Chem. Soc. 127*, 8594–8595. doi: 10.1021/ja050880n.

31. Holm, L., and Rosenström, P. (2010) Dali server: Conservation mapping in 3D, *Nucleic Acids Res. 38*. doi: 10.1093/nar/gkq366.

32. Ogura, H., Nishida, C. R., Hoch, U. R., Perera, R., Dawson, J. H., and Ortiz De Montellano, P. R. (2004) EpoK, a cytochrome P450 involved in biosynthesis of the anticancer agents epothilones A and B. Substrate-mediated rescue of a P450 enzyme, *Biochemistry 43*, 14712–14721. doi: 10.1021/bi048980d.

33. Pochapsky, T. C., Kazanis, S., and Dang, M. (2010) Conformational plasticity and structure/function relationships in cytochromes P450, *Antioxid. Redox Signal. 13*, 1273–1296. doi: 10.1089/ars.2010.3109.

34. Poulos, T.L., and Johnson, E. F. (2015) Structures of Cytochrome P450 Enzymes, in *Cytochrome P450*, pp 3–32. doi: 10.1007/0-387-27447-2_3.

35. Savino, C., Montemiglio, L. C., Sciara, G., Miele, A. E., Kendrew, S. G., Jemth, P., Gianni, S., and Vallone, B. (2009) Investigating the structural plasticity of a cytochrome P450. Three dimensional structures of P450 EryK and binding to its physiological substrate, *J. Biol. Chem. 284*, 29170–29179. doi: 10.1074/jbc.M109.003590.

36. Schlichting, I., Berendzen, J., Chu, K., Stock, A. M., Maves, S. A., Benson, D. E., Sweet, R. M., Ringe, D., Petsko, G. A., and Sligar, S. G. (2000) The Catalytic Pathway of Cytochrome P450Cam at Atomic Resolution, *Science 287(5458)*, 1615–1622. doi: 10.1126/science.287.5458.1615.

37. Guengerich, F. P. (2002) Cytochrome P450 enzymes in the generation of commercial products, *Nat. Rev. 1*, 359–366. doi:10.1038/nrd792.

38. Urlacher, V. B., and Girhard, M. (2012) Cytochrome P450 monooxygenases: An update on perspectives for synthetic application, *Trends Biotechnol. 30(1)*, 26-36. doi: 10.1016/j.tibtech.2011.06.012.

39. Bruno, R. D., and Njar, V. C. O. (2007) Targeting cytochrome P450 enzymes: a new approach in anti-cancer drug development, *Bioorg. Med. Chem. 15*, 5047–5060. doi: 10.1016/j.bmc.2007.05.046.

40. Lamb, D. C., Waterman, M. R., Kelly, S. L., and Guengerich, F. P. (2007) Cytochromes P450 and drug discovery, *Curr. Op. Biotech. 18*, 504–512. doi:10.1016/j.copbio.2007.09.010

41. Pikuleva, I. A., and Waterman, M. R. (2013) Cytochromes P450: Roles in diseases, *J. Biol. Chem. 288(24)*, 17091-17098. doi: 10.1074/jbc.R112.431916.

42. Schuster, I., and Bernhardt, R. (2007) Inhibition of cytochromes p450: existing and new promising therapeutic targets, *Drug Metab. Rev. 39*, 481–499. doi: 10.1080/03602530701498455.

43. Balding, P. R., Porro, C. S., McLean, K. J., Sutcliffe, M. J., Maréchal, J.-D., Munro, A. W., and de Visser, S. P. (2008) How do azoles inhibit cytochrome P450 enzymes? A density functional study, *J. Phys. Chem. A 112*, 12911–12918. doi: 10.1021/jp802087w.

44. Schulze, H., Hoa, G. H. B., and Jung, C. (1997) Mobility of norbornane-type substrates and water accessibility in cytochrome P-450(cam), *Biochim. Biophys. Acta - Protein Struct. Mol. Enzymol. 1338*, 77–92. doi:10.1016/S0167-4838(96)00192-6.

45. Carey, F. A., and Sundberg, R. J. (2007) Advanced Organic Chemistry Part B: Reactions and Synthesis, *Ebook*, pp 1–1199. ISBN-10: 0387683542.

46. Darban-Sarokhalil, D., Fooladi, A. A. I., Bameri, Z., Nasiri, M. J., and Feizabadi, M. M. (2011) Cytochrome CYP141: a new target for direct detection of Mycobacterium tuberculosis from clinical specimens, *Acta Microbiol. Immunol. Hung. 58*, 211–7. doi: 10.1556/AMicr.58.2011.3.4.

47. Lee, Y. T., Wilson, R. F., Rupniewski, I., and Goodin, D. B. (2010) P450cam visits an open conformation in the absence of substrate, *Biochemistry 49*, 3412–3419. doi: 10.1021/bi100183g.